

Supplementary Information

Influence of surface Sn species and hydrogen interactions on the OH groups formation over spherical silica-supported tin oxide catalysts

Sirawat Boonpai, Sippakorn Wannakao, Kongkiat Suriye, Victor Marquez, Joongjai Panpranot, Bunjerd Jongsomjit, Piyasan Praserthdam,* and Alexis T. Bell

Supplementary Information

Influence of surface Sn species and hydrogen interactions on the OH groups formation over spherical silica-supported tin oxide catalysts

Sirawat Boonpai, Sippakorn Wannakao, Kongkiat Suriye, Victor Marquez, Joongjai Panpranot, Bunjerd Jongsomjit, Piyasan Praserttham,* and Alexis T. Bell

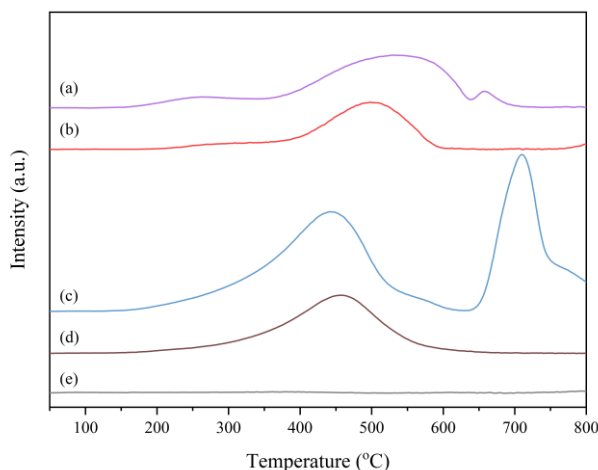


Figure S1. H₂-TPR profiles of SSP-supported Sn catalysts; IWI-10Sn (a), IWI-5Sn (b), Inc-10Sn (c), Inc-5Sn (d), SSP (e).

The reducibility of the SSP-supported Sn was investigated by the H₂-TPR as shown in Figure S1. In the temperature range studied (40-800 °C), all samples show the reduction peaks of Sn species on SSP support, excepting for the SSP support. There is no reduction peak below 800 °C on the SSP due to its nonreducible support property. In the low temperature range of 100-500 °C, there are two reduction peaks of Sn species on the impregnated catalysts (IWI-Sn) at around 250 °C and 480 °C, which is assigned to the reduction of small nano-sized SnO₂ species^{1,2}. Nevertheless, there are only one reduction peak of Sn species at around 440 °C on the incorporated catalysts (Inc-Sn) observed in the same temperature range of 100-500 °C. This indicates that the incorporation of Sn species into SSP are strongly interacted with support and are difficultly reduced to metallic Sn than those of the impregnated sample. In the high temperature range of 600-800 °C, the 10Sn/SSP and 10Sn-SSP show a high temperature reduction peak at around 640 and 725 °C, respectively, which is assigned to the reduction of crystalline SnO₂³. These results indicate that the crystalline SnO₂ species appear on high Sn content loading of IWI-10Sn and Inc-10Sn. The reduction peak of crystalline SnO₂ of Inc-10Sn is shifted to higher temperature than IWI-10Sn, indicating that Sn species are highly dispersed on catalyst surface Inc-Sn. These results are well consistent with the TEM and XRD results

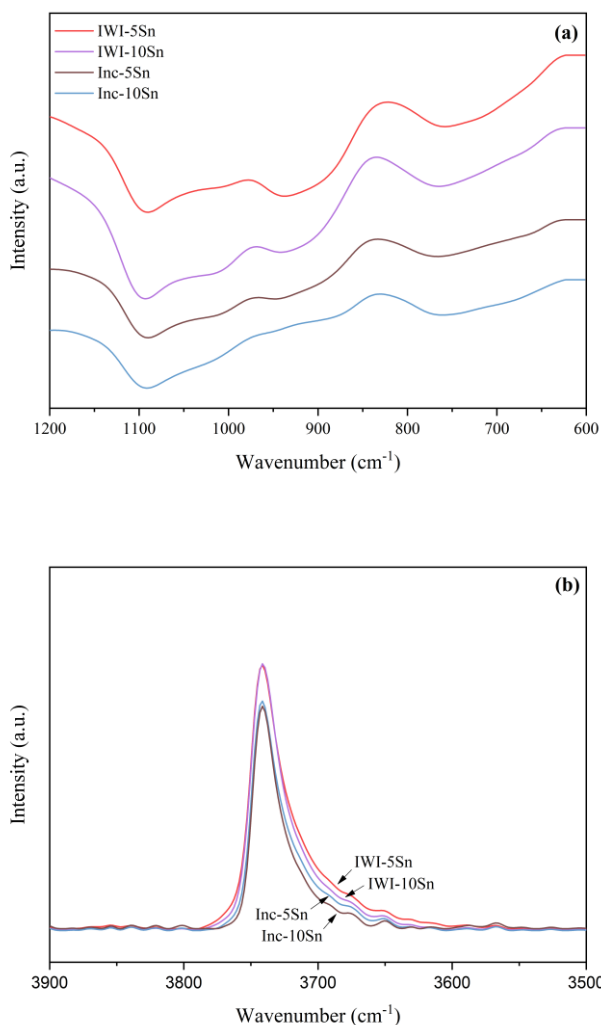


Figure S2. FT-IR spectra of SSP-supported Sn catalysts.

The FT-IR characterization was also used to analyze the existence of Sn species onto SSP framework as shown in Figure S2. The IR band at around 810 cm^{-1} , which is corresponded to the symmetric vibration modes of tetrahedral SiO_4 structure unit⁴, can be obviously observed on all samples. In addition, all samples also show the vibration peak at around 962 cm^{-1} corresponded to surface Sn–O–Si, suggesting the incorporation of Sn into the framework of pore walls in the silica support^{5, 6}. The previous studies reported that the direct evidence for the isomorphous substitution could be observed on the IR band at around $950\text{--}970\text{ cm}^{-1}$ ^{7, 8}. Comparing the intensity of all IR bands, it was found that the incorporated catalysts (Inc-Sn) exhibit lower intensity of all bands than the impregnated catalysts (IWI-Sn) due to the partial destruction of the ordered mesoporous structure on the incorporating of Sn species onto SSP. Moreover, it was also found that the intensity was decreased with increasing Sn content in both catalysts.

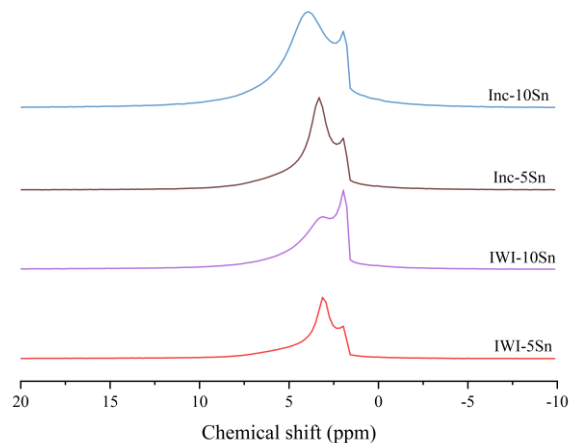


Figure S3. Solid state ^1H NMR spectra of SSP-supported Sn catalysts.

To obtain more information of the surface hydrogen on the SSP-supported Sn catalysts, the samples were investigated by ^1H MAS NMR as shown in Figure S3. Prior to investigation, the samples were pretreated with H_2/N_2 gas by the same step as done for the *in situ* DRIFTS experiments. The sharp signal at around 2.0 ppm was assigned to the terminal silanols on SiO_2 bulk and silica support appeared on all samples ⁹. It is interesting that all samples exhibited the peak around 2.8 ppm, ascribing to the hydrogen spillover adsorbed on Si–O–Si of the support ^{10, 11}. Therefore, it is further confirmed that the hydrogen spillover from tin oxide onto SSP support was essentially occurred. In addition, all samples also showed the peak at around 4.0 ppm, which ascribing to the hydroxyls Si–OH group. It is suggested that the further interaction between the adsorbed H species and Si–O–Si leads to the formation of Si–OH group ¹⁰. The capacity of this peak was in the following order: Inc-10Sn > Inc-5Sn > IWI-10Sn > IWI-5Sn, which is well consistent with the *in situ* DRIFTS and H_2 -TPD results.

Experimental

Material characterization

XRD pattern analysis was carried out using a D8 Advance of Bruker AXS using Ni-filter selecting $\text{CuK}\alpha$ radiation. Brunauer-Emmett-Teller (BET) surface areas, pore volumes and pore sizes of all catalysts were performed at $-196\text{ }^\circ\text{C}$ using a Micromeritics Chemisorb 2750 model ASAP 2000 automated system. Transmission electron microscopy (TEM) image, and energy-dispersive X-ray spectroscopy (TEM-EDS), which were obtained on a JEOL JEM-2010 microscope equipped with a LaB6 electron gun operated at 200 kV, were used to analyze the morphology and composition of the sample. Scanning electron microscopy (SEM) experiments were investigated on a Hitachi S3400N. The UV-vis DRS was recorded using Lambda 650 spectrophotometer in the range between 200 and 500 nm. The X-ray photoelectron spectroscopy (XPS) analysis was carried out using an AMICUS photoelectron spectrometer equipped with an $\text{Mg K}\alpha$ X-ray radiation operated at a voltage of 10 kV and a current of 20 mA. The Fourier transform infrared spectrometer (FT-IR) was recorded with a Bruker Vertex-70 FT-IR spectrometer equipped with a Harrick Praying Mantis attachment for diffuse reflectance spectroscopy using a Mercury-Cadmium-Telluride

(MCT) detector. The sample was performed in the *in situ* IR cell with KBr windows connected to the close circulating system. The sample was pretreated under mixed gas of H₂ flow (10 ml/min) and N₂ flow (10 ml/min) at 500 °C for 1 h, and then it was heated to 550 °C under a N₂ flow for 30 min, followed by cooling to 40 °C. The IR spectra were subtracted from the background spectrum obtained from KBr sample. The solid state ²⁹Si and ¹H NMR were determined by Fourier transform nuclear magnetic resonance spectrometer 400 MHz (Solid) using a Bruker AVANCE III HD (Ascend 400 WB) spectrometer using 4 mm MAS probes at a spin rate of 8 kHz. Hydrogen temperature-programmed reduction (H₂-TPR) analysis was performed to investigate reducibility of the sample. The measurement was carried out in a quartz microreactor by using the Micrometrics Chemisorbs 2750 automated system. The sample was pretreated in Ar (25 ml/min) at 500 °C for 1 h, and then cooled down to room temperature, then it was followed by a temperature-programmed reduction by 10% H₂ in Ar (15 ml/min) from room temperature to 800 °C with a heating rate of 10 °C/min. Hydrogen consumption was obtained by a thermal conductivity detector (TCD). Hydrogen temperature-programmed desorption (H₂-TPD) analysis was used to investigate the adsorption behavior of hydrogen. The sample was carried out in a quartz microreactor using the Micrometrics Chemisorbs 2750 automated system. The sample was pretreated with the mixed gas flow of H₂ (25 ml/min) and N₂ (25 ml/min) at 500 °C for 1 h, and then it was heated to 550 °C at a heating rate of 10 °C/min under a N₂ flow for 30 min. After that, the sample was cooled to 40 °C, followed by adsorption of H₂ gas flow for 30 min. Finally, the sample was purged with a N₂ flow for 1 h, and then it was heated to 400 °C at a heating rate of 10 °C/min under a N₂ flow. The signals of hydrogen desorption were monitored by a thermal conductivity detector.

References

1. H. Wang, H. Wang, X. Li and C. Li, *Appl. Surf. Sci.*, 2017, **407**, 456-462.
2. J. Dijkmans, M. Dusselier, W. Janssens, M. Trekels, A. Vantomme, E. Breynaert, C. Kirschhock and B. F. Sels, *ACS Catal.*, 2015, **6**, 31-46.
3. X. Wang and Y.-c. Xie, *Catal. Lett.*, 2001, **75**, 73-80.
4. X.-L. Yang, W.-L. Dai, H. Chen, J.-H. Xu, Y. Cao, H. Li and K. Fan, *Appl. Catal., A*, 2005, **283**, 1-8.
5. Q. Liu, M. Luo, Z. Zhao and Q. Zhao, *Chem. Eng. J.*, 2020, **380**.
6. Z. Liu, J. Zhou, K. Cao, W. Yang, H. Gao, Y. Wang and H. Li, *Appl. Catal., B*, 2012, **125**, 324-330.
7. V. Parvulescu, C. Anastasescu, C. Constantin and B.-L. Su, *Catal. Today*, 2003, **78**, 477-485.
8. B. Rakshe, V. Ramaswamy and A. Ramaswamy, *J. Catal.*, 1996, **163**.
9. D. Lenz, W. C. Conner Jr and J. Fraissard, *J. Catal.*, 1989, **117**.
10. L. Qian, W. Cai, L. Zhang, L. Ye, J. Li, M. Tang, B. Yue and H. He, *Appl. Catal., B*, 2015, **164**, 168-175.
11. Z. Chao, T. Wu, J. Ye, G. Chen and H. Wan, *Sci. China, Ser. B: Chem.*, 2001, **44**, 103-112.